Catalysis Today 161 (2011) 189–195

Contents lists available at ScienceDirect

Catalysis Today

journal homepage: www.elsevier.com/locate/cattod

Photocatalytic acetic acid decomposition leading to the production of hydrocarbons and hydrogen on Fe-modified TiO_2

Sylwia Mozia*, Aleksandra Heciak, Antoni W. Morawski

West Pomeranian University of Technology, Institute of Chemical and Environment Engineering, ul. Pułaskiego 10, 70-322 Szczecin, Poland

ARTICLE INFO

Keywords:
Photocatalysis
Hydrocarbons
Methane
Acetic acid
Fe/TiO_2

ABSTRACT

A photocatalytic generation of useful hydrocarbons and hydrogen from acetic acid under N_2 atmosphere is presented. The photocatalysts were prepared from a crude TiO_2 modified with $Fe(NO_3)_3$ and calcinated at the temperatures of 400–600 °C in argon atmosphere. The main gaseous products of CH_3COOH decomposition were CH_4 and CO_2. Moreover, ethane, propane and hydrogen were also detected. The most active photocatalyst towards CH_4 generation was TiO_2 containing 20 wt.% of Fe calcinated at 500 °C. The optimum loading of this photocatalyst was 1 g/dm^3. After 5 h of the process the amount of CH_4, CO_2, C_2H_6, C_3H_8 and H_2 evolved was 0.458, 0.450, 0.025, 0.003 and 0.013 mmol, respectively. An increase of CH_3COOH concentration from 0.01 to 1 mol/dm^3 resulted in an increase of methane production. A further increase of CH_3COOH concentration up to 10 mol/dm^3 led to a decrease of the process efficiency. The stability of the prepared photocatalysts against photocorrosion was very high. The amount of dissolved Fe did not exceed 0.17 wt.% of the total Fe present in a catalyst sample.

1. Introduction

Biogas has been recently considered to be an attractive source of clean energy. An increasing attention has been focused on developing new methods of methane or hydrogen production from renewable energy sources (e.g. biomass) to avoid the emission of greenhouse gases or other compounds responsible for air and water pollution. Photocatalytic conversion of organic matter leading to production of hydrogen or hydrocarbons might be an interesting solution for both, environmental and energy issues. Photocatalysis is especially attractive when wastewaters containing substances dangerous or toxic to bacteria are considered. In this case anaerobic digestion cannot be applied since methanogens are known to be tolerant to a small extent to many organic (e.g. phenols, alkanes, alcohols, ethers, ketones) and inorganic substances (e.g. heavy metals, ammonia) [1]. Photocatalysis, in general, is not (or almost not) specific and could be applied for any type of wastewaters, regardless of their toxicity [2].

TiO_2 is a commonly applied photocatalyst because of its significant activity, high stability and low cost. Most of the already published papers [3–8] describe photocatalytic production of CH_4 in gas phase under UV light in the presence of pure or modified TiO_2. In 1970's Kraeutler and Bard [9–11] published a series of papers reporting photocatalytic decarboxylation of acetic acid (photo-Kolbe reaction) in the presence of Pt/TiO_2 catalyst. The main products of this reaction were CH_4 and CO_2. Since that time a few more reports concerning production of CH_4 from aliphatic acids and alcohols have been published [5–13]. Nevertheless, literature data related to the photocatalytic generation of methane in liquid phase are very limited.

Titania photocatalysis faces several significant limitations because of high energy band gap of TiO_2, recombination of e^-/h^+ pairs and low interfacial charge transfer [14]. The literature data [14–21] show that modification of TiO_2 with Fe can improve its photoactivity by increasing UV-light absorption capability; inhibition of rutile phase formation or acting as both e^-/h^+ traps to reduce their recombination rate [16]. According to literature data a proper concentration of Fe has a crucial influence on catalyst photoactivity but there are no publications concerning the application of Fe/TiO_2 in photo-Kolbe reaction. There are numerous reports describing the usage of Fe/TiO_2 for degradation of organics in which photocatalysts with Fe loading as low as 0.05 at.% [20] or as high as 50 at.% [18] were applied. In general, Fe-modified samples can be divided into low-loaded (or doped) [15–17,19,22] and heavy-loaded (or composite) [18,19,21,23] ones. Heavy-loaded Fe/TiO_2 photocatalysts were investigated to a lesser extent than the doped ones. However, the photocatalytic activity [18] of the former catalysts as well as their stability in terms of photocorrosion [19] has been proved. For that reasons during the present research we have focused on the heavy-loaded Fe/TiO_2.

During the present investigations different TiO_2 powders modified with $Fe(NO_3)_3$ were applied for photocatalytic generation of useful hydrocarbons (mainly methane) and H_2 from CH_3COOH

* Corresponding author. Tel.: +48 91 449 47 30; fax: +48 91 449 46 86.
E-mail addresses: sylwia.mozia@zut.edu.pl, sylwiam@ps.pl (S. Mozia), aheciak@zut.edu.pl (A. Heciak), amor@zut.edu.pl (A.W. Morawski).

0920-5861/$ – see front matter © 2010 Elsevier B.V. All rights reserved.
doi:10.1016/j.cattod.2010.09.020

under N_2 atmosphere. Acetic acid was selected as a model compound due to the fact that it undergoes the so-called photo-Kolbe reaction. The products of this reaction are CH_4 and CO_2. This means that the gaseous mixture obtained during the photocatalytic reaction has a composition similar to that of biogas obtained by a conventional anaerobic digestion method. Another reason for the application of CH_3COOH as a model compound is that its presence amongst by-products of photodegradation of most organic substances is commonly observed.

2. Materials and methods

2.1. Photocatalysts

The photocatalysts were prepared from crude TiO_2 obtained directly from the production line (sulfate technology) at the Chemical Factory "Police" (Poland). A defined amount of TiO_2 was introduced into a beaker containing aqueous solution of $Fe(NO_3)_3$ and stirred for 22 h. After that water was evaporated, the samples were dried at 80 °C for 24 h in an oven, and then calcinated at 400, 500 or 600 °C in Ar atmosphere for 1 h (83 dm^3/min). The amount of Fe introduced to the samples was 10, 20 or 30 wt.%. The samples modified with $Fe(NO_3)_3$ were denoted as A-FeXNY, where X refers to Fe content (10–30 wt.%) and Y to the calcination temperature (400–600 °C). In order to compare the results crude TiO_2 without any modifying agent was calcinated at 500 °C for 1 h (A-500). Moreover, the commercial TiO_2 AEROXIDE® P25 (Evonik, Germany) was also used.

2.2. Characterization of photocatalysts

The XRD patterns were recorded using X'Pert PRO diffractometer with CuKα radiation (λ = 1.54056 Å). The average anatase crystallite diameter was calculated using Scherrer's equation [17,24].

The UV–vis/DR spectra were recorded using Jasco V530 spectrometer (Japan) equipped with an integrating sphere accessory for diffuse reflectance spectra. $BaSO_4$ was used as the reference.

The Brunauer–Emmett–Teller (BET) surface area of the powders was determined on the basis of nitrogen adsorption–desorption measurements at 77 K conducted in Quadrasorb SI (Quantachrome, USA) apparatus. All of the samples were degassed at 80 °C prior to measurements.

The concentration of Fe released from the Fe/TiO_2 photocatalysts to the CH_3COOH solution was determined using colorimetric method with 1,10-phenanthroline.

2.3. Photocatalytic reaction

The photocatalytic reaction was conducted in a cylindrical glass reactor (Heraeus, type UV-RS-2, $V = 765\ cm^3$) equipped with a medium pressure mercury vapour lamp (TQ-150, $\lambda_{max} = 365$ nm, $I = 146\ W/m^2$). In the upper part of the reactor a gas sampling port was placed. At the beginning of the experiment 0.35 dm^3 of CH_3COOH solution (0.01 (pH 3.6), 0.1 (pH 3.0), 1 (pH 2.6) or 10 (pH 1.8) mol/dm^3) and a defined amount of a catalyst (0.175, 0.35, 0.525 or 0.7 g) were introduced into the reactor. Before the photocatalytic reaction N_2 was bubbled through the reactor for at least 1 h to ensure that the dissolved oxygen was eliminated. Then, the N_2 flow was stopped and UV lamp was turned on to start the photoreaction. The process was conducted for 5 h. The reaction mixture was continuously stirred during the experiment by means of a magnetic stirrer. The reaction temperature was 25 °C. Additionally, two blind tests: (a) without photocatalyst and (b) in the dark were also conducted.

All the experiments were repeated at least twice. The presented data are mean values obtained from the two experiments (S.D. were below 8%). Gaseous products were analyzed using GC SRI 8610C equipped with TCD and HID detectors, and Shincarbon, molecular sieve 5A and 13X columns. Helium was used as the carrier gas. The composition of the liquid phase was determined using GC SRI 8610C equipped with FID detector and MXT®-1301 column. Hydrogen was used as the carrier gas.

3. Results and discussion

3.1. Physico-chemical properties of the photocatalysts

Fig. 1 shows XRD patterns of the TiO_2 and Fe/TiO_2 photocatalysts. The phase composition of the photocatalysts is presented in Table 1. It can be observed that crude TiO_2 contained anatase and rutile phases in the ratio of 85:15. The diffraction lines were weak and broad suggesting poor crystallinity of the sample. The crystallite size of anatase in the crude TiO_2 was 7 nm. The heat treatment of crude TiO_2 (A-500) resulted in an improvement of TiO_2 crystallinity associated with anatase crystals growth (12 nm vs. 7 nm, Table 1). The crystallite size of anatase in the Fe/TiO_2 samples was in the range of 8–15 nm. The thermal treatment did not significantly affect the crystallite size of anatase, especially in case of the samples calcinated at 400–500 °C. Samples A-Fe10N500, A-Fe20N500 and A-Fe30N500 annealed at 500 °C exhibited crystallinity similar to that of crude TiO_2. Moreover, anatase crystals of these powders were a little smaller than in case of A-500 (9 nm vs. 12 nm). These results indicate that Fe introduced in the form of $Fe(NO_3)_3$ did not catalyse anatase crystallites growth upon annealing. The obtained data are consistent with the results presented by Ranjit et al. [22]. The presence of weak diffraction lines of anatase as well as lower anatase crystallinity in case of Fe/TiO_2 samples might be attributed to the fine dispersion of iron in titanium dioxide restricting crystallite growth [18,19].

Moreover, the obtained data suggest that the type and properties of the products obtained during modification of TiO_2 with $Fe(NO_3)_3$ depended on the Fe concentration and calcination temperature. In case of the samples containing 20 and 30 wt.% of Fe, iron oxide (Fe_2O_3) was identified. It can be seen (Fig. 1) that either an increase of annealing temperature in case of the catalysts containing 20 wt.% of Fe or introduction of a higher amount of Fe was responsible for growth of crystallite size of Fe_2O_3 (narrowing of diffraction lines). The lack of diffraction lines of Fe_2O_3 in case of the

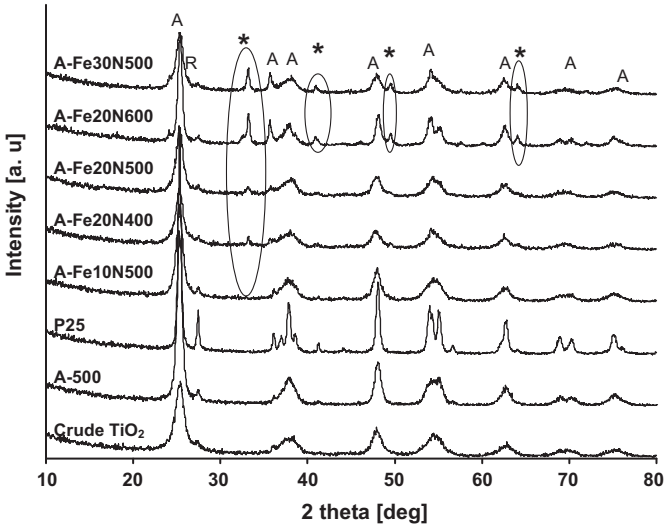

Fig. 1. XRD patterns of photocatalysts: (A) anatase, (R) rutile, and (*) Fe_2O_3.

Table 1
Physico-chemical properties of the photocatalysts.

Sample	Specific surface area S_{BET} [m^2/g]	Phase composition by XRD	Crystallite size of anatase [nm]	Anatase over rutile ratio (A:R)
Crude TiO_2	215	A, R	7	85:15
A-500	103	A, R	12	92:8
P25	50	A, R	22	82:18
A-Fe10N500	109	A, R	9	89:11
A-Fe20N400	109	A, R, Fe_2O_3	8	85:15
A-Fe20N500	82	A, R, Fe_2O_3	9	87:13
A-Fe20N600	44	A, R, Fe_2O_3	15	93:7
A-Fe30N500	83	A, R, Fe_2O_3	9	87:13

A; anatase; R: rutile.

XRD pattern of A-Fe10N500 might be attributed to the amorphous nature of Fe_2O_3 or too low amount of this phase to be detected using XRD method.

UV–vis/DR spectra (Fig. 2) of Fe/TiO_2 powders indicate that the light absorption characteristics of TiO_2 were affected by the presence of Fe. A significant increase in the absorption at $\lambda > 400$ nm was observed for the Fe/TiO_2 samples. The absorption in the visible range was stronger at higher Fe concentrations. A similar phenomenon was observed by Ambrus et al. [25]. The absorption spectra of Fe/TiO_2 were red shifted compared to those of pure titania. The red shift could be attributed to a charge transfer transition between Fe and TiO_2 conduction or valence bands [26].

A specific BET surface area (S_{BET}) of the pure titania samples decreased with increasing calcination temperature from 215 m^2/g in case of crude TiO_2 to 103 m^2/g for A-500 (Table 1). In case of Fe/TiO_2, the S_{BET} decreased with the annealing temperature from 109 m^2/g for A-Fe20N400 to 44 m^2/g for A-Fe20N600. Moreover, it could be observed that S_{BET} of A-500, A-Fe20N400 and A-Fe10N500 were comparable (103 vs. 109 m^2/g), whereas samples containing 20 and 30 wt.% of Fe calcinated at 500 °C had lower S_{BET}. These results show that the presence of Fe compounds strongly affects the surface area of the photocatalysts. A decrease of S_{BET} with increasing annealing temperature in case of catalysts containing 20 wt.% of Fe might be attributed to growing crystallite size of anatase and Fe_2O_3 (Table 1).

3.2. Photocatalytic decomposition of acetic acid in the presence of different photocatalysts

The P25, crude and annealed TiO_2 as well as the Fe/TiO_2 photocatalysts were applied for the photocatalytic decomposition of CH_3COOH under N_2 atmosphere. The catalyst loading amounted to 1 g/dm^3 and the initial concentration of CH_3COOH was 1 mol/dm^3. The solution pH was equal to pH 2.6 and was constant during the whole process. The effectiveness of hydrocarbons and hydrogen generation was evaluated on the basis of the amounts of the gases

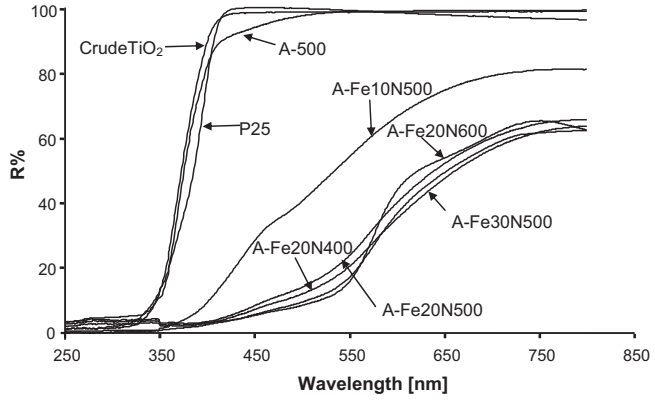

Fig. 2. UV–vis/DR spectra of different photocatalysts.

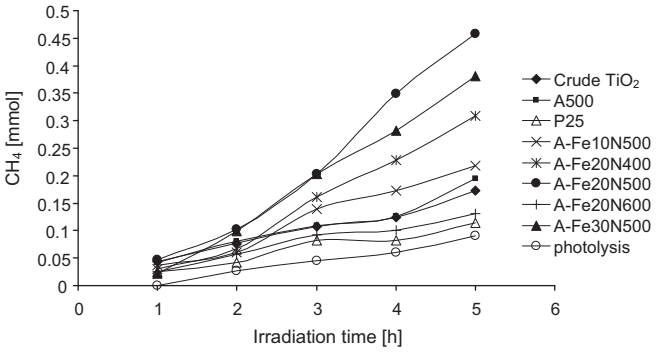

Fig. 3. Evolution of CH_4 in time of irradiation. Photocatalysts loading: 1 g/dm^3; CH_3COOH concentration: 1 mol/dm^3.

which evolved to the headspace volume of the reactor. Regardless of the photocatalyst used, the gaseous products identified were CH_4, CO_2, C_2H_6, C_3H_8 and H_2. When a blank test in the dark was conducted, no reaction products were identified showing that UV light is necessary for the reaction to occur.

3.2.1. Hydrocarbons production from acetic acid

Before the photocatalytic experiments a blank test in the absence of photocatalyst (photolysis) was conducted (Figs. 3 and 4). The formation of CH_4, CO_2 and C_2H_6 was observed. However, the amount of the gases was very low (0.086, 0.090 and 0.004 mmol, respectively). Therefore, it could be stated that the results obtained in the presence of photocatalysts, which are discussed below, are mainly due to photocatalytic, not photolytic reaction pathway.

Methane formation during the photocatalytic decomposition of CH_3COOH follows the so-called photo-Kolbe reaction pathway. The main products of this reaction are CH_4 and CO_2 [9–12]:

$$CH_3COOH + h^+ \rightarrow CH_3^{\bullet} + CO_2 + H^+ \quad (3)$$

Reaction (3) represents the photocatalytic decarboxylation of CH_3COOH initiated by photogenerated holes.

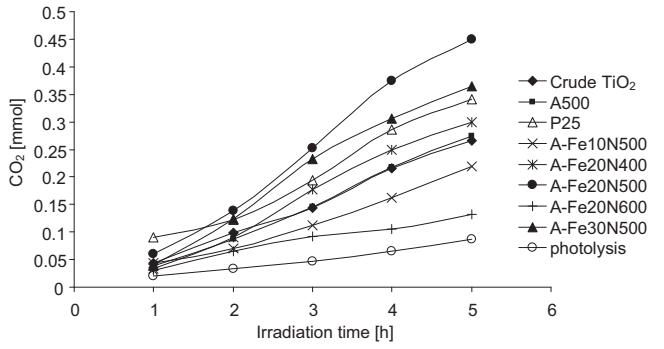

Fig. 4. Evolution of CO_2 in time of irradiation. Photocatalysts loading: 1 g/dm^3; CH_3COOH concentration: 1 mol/dm^3.

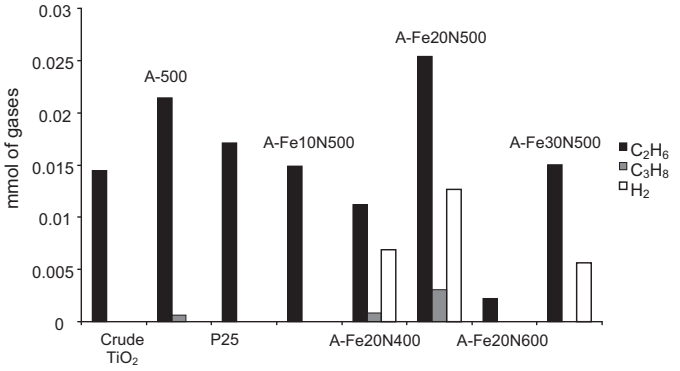

Fig. 5. Comparison of the amount of C_2H_6, C_3H_8 and H_2 evolved after 5 h of irradiation in the presence of different photocatalysts. Photocatalysts loading: 1 g/dm^3; CH_3COOH concentration: 1 mol/dm^3.

The reaction of ethane formation can be presented as follows [12]:

$$2CH_3COOH \rightarrow C_2H_6 + 2CO_2 + H_2 \quad (4)$$

or, taking into consideration the recombination of methyl radicals [4]:

$$CH_3^\bullet + CH_3^\bullet \rightarrow C_2H_6 \quad (5)$$

In the same way the reaction of propane formation could be written.

Figs. 3 and 4 show the amounts of CH_4 and CO_2 produced as a function of irradiation time. The amounts of both gases continuously increased during the process. After 5 h the amount of CH_4 was in the range of 0.114–0.458 mmol (Fig. 3). The highest yield of methane evolution was observed for A-Fe20N500 and the lowest one for P25. The amount of CO_2 after 5 h of irradiation ranged from 0.132 to 0.450 mmol (Fig. 4). The lowest amount of CO_2 was produced in case of A-Fe20N600, whereas the highest one in the presence of A-Fe20N500.

As was mentioned earlier, amongst the gaseous products of the reaction ethane and propane were also identified. In general, the amounts of C_2H_6 and C_3H_8 were significantly lower compared to those of CH_4 and CO_2 (Fig. 5). The amount of C_2H_6 after 5 h of irradiation was in the range of 0.002–0.025 mmol. The highest yield of ethane evolution was observed for A-Fe20N500, whereas the lowest one for A-Fe20N600. Propane was identified only in case of A-500, A-Fe20N400 and A-Fe20N500. At the end of irradiation the amount of C_3H_8 was found to be in the range of 0.001–0.003 mmol. The highest effectiveness of propane generation was observed in case of A-Fe20N500. The reason for which propane evolution in case of TiO_2, P25, A-Fe10N500, A-Fe20N600 and A-Fe30N500 was not detected could be lower photoactivity of these samples towards production of all gases from CH_3COOH. A lengthening of irradiation time would probably result in the evolution of C_3H_8 to a gas phase.

The presented data show that the efficiency of transformation of CH_3COOH to CH_4 calculated after 5 h of irradiation was about 0.033–0.13%, depending on the photocatalyst. However, it should be noticed that the process was conducted for 5 h only while the time necessary for a complete decomposition of CH_3COOH at the applied concentration (1 mol/dm^3) is significantly longer. Taking into consideration that the concentration of CH_4 was continuously increasing in time, it could be supposed that the transformation efficiency at longer times would be higher.

The yields of ethane and propane evolution were significantly lower than that of methane, what clearly indicates that the reactions (4) and (5) are of minor importance.

From the reaction (3) it could be found that every mole of CH_3COOH gives one mole of CH_4 and one mole of CO_2, i.e. CH_4/CO_2 ratio should be equal to 1. However, in the performed experiments CH_4/CO_2 ratio differed from unity, especially in case of pure TiO_2. The CH_4/CO_2 ratio calculated after 5 h of irradiation was equal to 0.65, 0.71 and 0.34 for crude TiO_2, A-500 and P25, respectively and 0.99, 1.03, 1.02, 0.99, 1.04 for A-Fe10N500, A-Fe20N400, A-Fe20N500, A-Fe20N600 and A-Fe30N500, respectively. Taking into consideration the gases solubility, the concentration of CO_2 in gaseous phase should be a little lower than that of CH_4. When the amount of CO_2 evolved from the solution is higher than that of methane, some other reactions, besides the photo-Kolbe reaction, have to be taken into consideration. CO_2 is also generated in reactions leading to ethane and propane formation. However, since the amounts of both gases were very low, it is rather doubtful that such a high concentration of CO_2 as observed in case of pure titania, (especially P25) was produced in these reactions.

The formation of greater amounts of CO_2 than CH_4 during decomposition of CH_3COOH is not a new topic. There were several reports about that phenomenon during the last 30 years, nevertheless none of them explicated it clearly [12,27–29]. Sakata et al. [12] suggested that CO_2/CH_4 ratio $\neq$ 1 might be an effect of organic acids oxidation but no reasonable mechanism was proposed. Yoneyama et al. [27] claimed that yielding CO_2 as the main product could result from degradation of ethanol or acetaldehyde, being by-products of CH_3COOH decomposition. However, the authors concluded that CO_2 formation would always be correlated with a greater evolution of H_2 which did not occur in our system (see Section 3.2.2). Moreover, formation of hydroxyl radicals in competition with methyl radicals was proposed [27]. $^\bullet OH$ radicals might be involved in the reaction leading to a generation of CO_2 [27]. On the basis of the results obtained in the present study it was supposed that an excess of CO_2 originated from the mineralization of acetic acid to H_2O and CO_2. A very high photocatalytic activity of P25 in degradation and mineralization of organic compounds is well known and widely described in literature. Efficient formation of hydroxyl radicals, being the main oxidizing species during photocatalytic reaction, is responsible for the high photoactivity of P25. However, direct oxidation of CH_3COOH takes place in the presence of O_2 not $^\bullet OH$ [27]:

$$CH_3COOH + 2O_2 \rightarrow 2CO_2 + 2H_2O \quad (6)$$

$$CH_3COOH + OH^\bullet \rightarrow CH_3^\bullet + CO_2 + H_2O \quad (7)$$

Therefore, since no atmospheric oxygen was present in the system, the involvement of photogenerated oxygen should be considered [30,31]:

$$OH^\bullet + OH^\bullet \rightarrow H_2O_2 \quad (8)$$

$$H_2O_2 + 2h^+ \rightarrow O_2 + 2H^+ \quad (9)$$

$$H_2O_2 + OH^\bullet \rightarrow H_2O + HO_2^\bullet \quad (10)$$

$$HO_2^\bullet + OH^\bullet \rightarrow H_2O + O_2 \quad (11)$$

$$HO_2^\bullet + H^+ + e^- \rightarrow H_2O_2 \quad (12)$$

$$2H_2O_2 \rightarrow 2H_2O + O_2 \quad (13)$$

According to Eq. (6) a reaction of CH_3COOH with photogenerated oxygen would lead to its mineralization to CO_2 and H_2O.

It could not be excluded that mineralization of CH_3COOH took place also in the presence of other samples. However, since CH_4/CO_2 ratio in case of Fe/TiO_2 was close to 1 it could be supposed that the photo-Kolbe reaction pathway was the primary one in the presence of these catalysts.

In order to clarify the reaction mechanism it is important to identify the products in the aqueous medium besides those in the gaseous phase. The main compounds detected in the liquid phase during photocatalytic decomposition of acetic acid

were methanol (CH_3OH), acetone ($CO(CH_3)_2$) and acetaldehyde (CH_3CHO). Regardless of the photocatalyst, the concentration of acetone was the highest from all the liquid products identified; however, it remained very low (<1.5 μmol/dm^3). Since $^{\bullet}OH$ radicals are known to have a strong oxidation power and can easily oxidize various organic compounds, the presence of reaction products in a liquid phase is explained reasonably by assuming the involvement of these radicals [12]:

$$CH_3^{\bullet} + OH^{\bullet} \rightarrow CH_3OH \quad (14)$$

$$CH_3OH + CH_3COOH \rightarrow CH_3COOCH_3 + H_2O \quad (15)$$

$$C_2H_5^{\bullet} + OH^{\bullet} \rightarrow C_2H_5OH \quad (16)$$

$$C_2H_5OH + 2OH^{\bullet} \rightarrow CH_3CHO + 2H_2O \quad (17)$$

Some organic intermediates, e.g. methanol might be further decomposed to form CO_2 and H_2 [12]:

$$CH_3OH + H_2O \rightarrow CO_2 + 3H_2 \quad (18)$$

Other compounds, such as acetaldehyde, might be further mineralized yielding CO_2 as a product [32,33]:

$$CH_3CHO + 3H_2O + 10h^+ \rightarrow 2CO_2 + 10H^+ \quad (19)$$

In view of the above it could be concluded that photogenerated $^{\bullet}OH$ radicals and oxygen might lead to the formation of organic intermediates in the liquid phase, their further decomposition as well as to direct mineralization of CH_3COOH.

On a basis of the results obtained at the end of irradiation the activity of the photocatalysts towards methane generation can be put in the following order: A-Fe20N500 > A-Fe30N500 > A-Fe20N400 > A-Fe10N500 > A-500 > crude TiO_2 > A-Fe20N600 > P25. Comparing these data with the S_{BET} of the photocatalysts (Table 1) it could be concluded that S_{BET} did not influence the activity of photocatalysts towards CH_4 formation. For example, A-Fe20N400, having higher S_{BET} than A-Fe20N500 (109 vs. 82 m^2/g) exhibited lower activity in CH_4 generation than the latter sample. Other potentially important parameters, such as anatase over rutile ratio and crystallinity did not obviously influence the activity either. Samples A-500 and A-Fe20N600 had similar crystallite size of anatase and anatase over rutile ratio (12 vs. 15 and 92:8 vs. 93:7, respectively) but showed different effectiveness towards CH_4 generation. These results suggest that the main parameter responsible for the activity of TiO_2 in the photo-Kolbe reaction was Fe content. From the obtained results a conclusion can be drawn that the highest effectiveness of CH_4 evolution was in case of A-Fe20N500. The high photocatalytic activity of this catalyst might be attributed to the presence of Fe_2O_3 phase (Fig. 1) in a suitable ratio. According to Hung et al. [16] the improved activity of Fe/TiO_2 could be due to reduction of the recombination rate of h^+/e^- pairs during the photodegradation. This phenomenon seems to be crucial in case of the obtained results. In a composite semiconductor, such as TiO_2–Fe_2O_3, photogenerated electrons can be transferred from the conduction band of TiO_2 and accumulated in the conduction band of Fe_2O_3, whereas holes could accumulate in the valence band of iron oxide. The recombination of h^+/e^- pairs competes with the reaction of these charge carriers with the appropriate species present in the solution. The discussed process is conducted in the absence of oxygen, therefore one might suppose that the recombination will proceed with a high rate. However, since acetic acid, being a hole scavenger is present in the reaction mixture, holes from the valence band of TiO_2 are scavenged by CH_3COOH which undergoes the photo-Kolbe reaction. In this case Fe_2O_3 acts as the electron trap while CH_3COOH as the hole scavenger. Therefore, the h^+/e^- recombination rate can be reduced and the photoactivity of the Fe-modified catalysts towards the photo-Kolbe reaction can be enhanced.

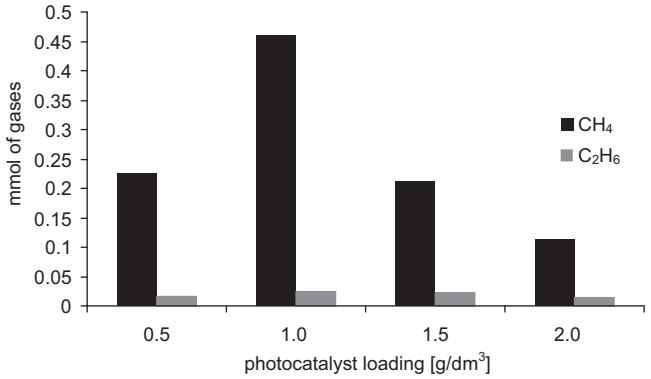

Fig. 6. Comparison of the amount of CH_4 and C_2H_6 evolved after 5 h of irradiation. Photocatalyst: A-Fe20N500; photocatalyst loadings: 0.5, 1, 1.5 and 2 g/dm^3; CH_3COOH concentration: 1 mol/dm^3.

Above 20 wt.% of Fe, the activity towards CH_4 formation slightly decreased (A-Fe30N500). The most reasonable explanation for that could be high coverage of TiO_2 particles with Fe_2O_3 resulting in a reduction of the accessibility of titania surface to CH_3COOH molecules. Moreover, electrons and holes can be derived to the Fe_2O_3 phase, setting the energy levels of the conduction or valence band to inadequate values for charge transfer to adsorbed substrate but also to promoting h^+/e^- recombination [19]. This results in a decrease of the reaction efficiency. And vice versa, Fe amount of 10 wt.% was too low to significantly improve the effectiveness of methane generation.

3.2.2. Hydrogen production from acetic acid

In case of A-Fe20N400, A-Fe20N500 and A-Fe30N500, hydrogen was also detected among other gaseous products of the process (Fig. 5). The photocatalytic evolution of hydrogen in the presence of sacrificial agents has been already described in the literature [12,30,34–37]. In general, when a reducing agent, or hole scavenger, such as alcohol [34–37] or organic acid [12,34] is present in the solution, hydrogen production can be observed.

The highest yield of hydrogen evolution was observed for A-Fe20N500 (0.013 mmol, Fig. 5). High photoactivity of this sample towards H_2 production compared to other catalysts is probably associated with the presence of Fe. Khan et al. [17] reported that well and uniform dispersed iron in the bulk of TiO_2 can capture photoinduced electrons, resulting in much improved hydrogen production in case of Fe/TiO_2 compared to pure titania.

The evolution of hydrogen was significantly lower than that of CH_4 or CO_2, even in case of Fe/TiO_2. The reason for that could be acidic pH of the reaction environment. It was reported that H_2 production is favored in neutral or basic solutions [34]. The presence of H_2 was not observed in case of crude TiO_2, P25, A-500, A-Fe10N500, A-Fe20N600 and A-Fe30N500 which was probably due to generally lower photoactivity of these samples in the investigated process. However, it could be supposed that, as for propane, a lengthening of the reaction time would lead to H_2 evolution in the presence of these catalysts as well.

3.3. Effect of A-Fe20N500 loading on process efficiency

To determine the influence of photocatalyst loading on the hydrocarbons production rate, various amounts of A-Fe20N500 (0.5, 1.0, 1.5 or 2.0 g/dm^3) were introduced into CH_3COOH solution (1 mol/dm^3). Fig. 6 shows the amounts of methane and ethane evolved after 5 h of irradiation. The amount of CH_4 was in the range of 0.112–0.458 mmol, whereas the amount of C_2H_6 ranged from 0.014 to 0.025 mmol. Moreover, CO_2 was also detected at the amount of 0.139–0.450 mmol. C_3H_8 and H_2 were identified only

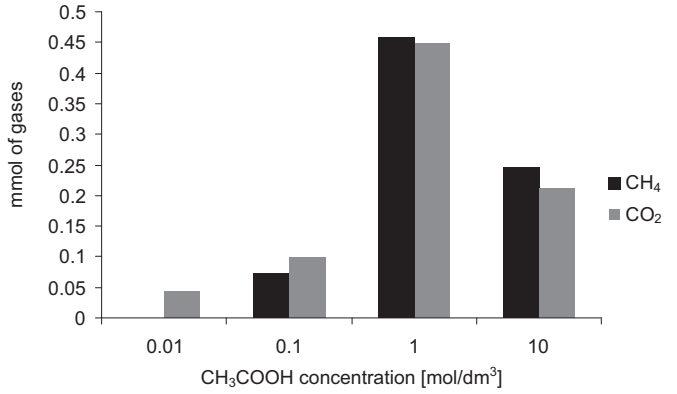

Fig. 7. Comparison of the amount of CH_4 and CO_2 evolved after 5 h of irradiation. Photocatalyst: A-Fe20N500; photocatalyst loading: 1 g/dm^3; CH_3COOH concentrations: 0.01, 0.1, 1 and 10 mol/dm^3.

in case of the catalyst concentration of 1 g/dm^3. The obtained data show that the most adequate catalyst loading was 1 g/dm^3. The concentration of 0.5 g/dm^3 was too low to obtain high hydrocarbons production rate, whereas at loadings higher than 1 g/dm^3 a decrease in the reaction rate was observed. The reason for that was a reduction of light penetration in the reactor and/or agglomeration of catalyst particles resulting in a decrease of surface area of the catalyst available for CH_3COOH molecules [38,39].

3.4. Effect of CH_3COOH concentration on process efficiency

During photodegradation of organic compounds an increase of the degradation rate with increasing reactant concentration is usually observed to a certain level. Then, due to saturation of the catalyst surface the reaction rate becomes independent of the reactant concentration and reaches a steady value within a certain range of concentrations [40]. A further increase of the reactant concentration leads to a decrease of the degradation rate [31]. An excessively high concentration of organic substrates is known to simultaneously saturate the photocatalyst surface and reduce the photonic efficiency leading to photocatalyst deactivation [41].

During the experiments the following CH_3COOH concentrations were applied: 0.01, 0.1, 1 and 10 mol/dm^3. A-Fe20N500 (1 g/dm^3) was used as the photocatalyst due to its highest activity from all the samples used. Fig. 7 presents the results obtained after 5 h of irradiation.

In case of the lowest concentration of CH_3COOH only CO_2 was detected (0.044 mmol). At 0.1 mol/dm^3 the formation CH_4 (0.074 mmol), CO_2 (0.099 mmol) and C_2H_6 (0.019 mmol) was observed. Hydrogen and propane were not produced. The highest effectiveness of the gases formation was observed in case of 1 mol/dm^3 CH_3COOH solution. A further increase of CH_3COOH concentration up to 10 mol/dm^3 led to a decrease in the production rate of the gases. The amount of CH_4, CO_2, C_2H_6, C_3H_8 and H_2 evolved in this case was equal to 0.245, 0.212, 0.021, 0.001 and 0.004 mmol, respectively. The obtained results illustrate well the dependence of the reaction rate on the reactant concentration which was discussed earlier.

3.5. Photocorrosion of the Fe-modified photocatalysts

A very important factor in case of Fe/TiO_2 is the stability of the photocatalysts. Photocorrosion of Fe-modified titania has already been reported in literature [19,42]. The photodissolution of a photocatalyst is undesirable because it can lead to its inactivation.

In view of the above the concentration of total iron released in the reaction mixture was measured at the end of each experiment. In general, it was observed that the amount of dissolved Fe did not exceed 0.17 wt.% of the total Fe in a catalyst sample. In case of the photocatalysts calcinated at 500 °C the highest amount of iron dissolved in the solution was found when A-Fe10N500 was used (0.17 wt.%). For the other two samples (A-Fe20N500 and A-Fe30N500) the amount of the released Fe was comparable and amounted to ca. 0.09 wt.%. The influence of calcination temperature on the photodissolution was also observed. With increasing the temperature more stable samples were obtained, although the differences were not very significant. The amount of iron released from the catalysts containing 20 wt.% of Fe and calcinated at 400, 500 and 600 °C was 0.12, 0.09 and 0.06 wt.%, respectively. The obtained results show that the stability of the prepared photocatalysts against photocorrosion was very high. Navío et al. [19] concluded that heavy-loaded samples are more stable because of the presence of hematite Fe_2O_3 which is probably less easily photocorroded. This conclusion was supported by the results obtained during the present research.

4. Conclusions

The gaseous products identified during the photocatalytic decomposition of CH_3COOH were CH_4, CO_2, C_2H_6, C_3H_8 and H_2 although the occurrence of these gases depended on the catalyst used. In all the experiments CH_4 and CO_2 were obtained at the highest amount.

In case of Fe/TiO_2 the effectiveness of hydrocarbons and hydrogen generation was influenced mainly by the amount of Fe. The most active photocatalyst towards all the identified gases production was A-Fe20N500. The highest yield of the gases evolution was obtained for 1 g/dm^3 of A-Fe20N500 and 1 mol/dm^3 of CH_3COOH.

The high photocatalytic activity of A-Fe20N500 was attributed to the presence of Fe_2O_3 in a suitable ratio and its good crystallinity associated with annealing temperature. In the investigated process Fe_2O_3 acts as the electron trap while CH_3COOH as the hole scavenger. Therefore, the h^+/e^- recombination rate can be reduced and the photoactivity of the Fe-modified catalyst towards the photo-Kolbe reaction can be enhanced.

The stability of the prepared photocatalysts against photocorrosion was very high. The amount of dissolved Fe did not exceed 0.17 wt.% of the total Fe present in a catalyst sample and was the highest in case of A-Fe10N500.

The obtained results show that photocatalytic decomposition of acetic acid under UV irradiation could be a promising method of producing "photo-biogas" containing useful hydrocarbons, mainly methane. However, since the yield of methane and other hydrocarbons production was low, further investigations are necessary in order to improve the process efficiency.

Acknowledgement

This work has been supported by the Polish Ministry of Science and Higher Education as a scientific project N N523 413435 (2008–2011).

References

[1] Y. Chen, J.J. Cheng, K.S. Creamer, Bioresour. Technol. 99 (2008) 4044–4064.
[2] V. Augugliaro, M. Litter, L. Palmisano, J. Soria, J. Photochem. Photobiol. C 7 (2006) 127–144.
[3] K. Koči, L. Obalová, Z. Lacný, Chem. Pap. 62 (2008) 1–9.
[4] M. Subrahmanyam, S. Kaneco, N. Alonso-Vante, Appl. Catal. B 23 (1990) 169–174.
[5] Y. Ku, W.H. Lee, W.Y. Wang, J. Mol. Catal. A: Chem. 212 (2004) 191–196.
[6] S.S. Tan, L. Zou, E. Hu, Sci. Tech. Adv. Mater. 8 (2007) 89–92.
[7] S.S. Tan, L. Zou, E. Hu, Catal. Today 115 (2006) 269–273.
[8] M. Anpo, H. Yamashita, Y. Ichihashi, S. Ehara, J. Electroanal. Chem. 396 (1995) 21–26.

[9] B. Kraeutler, A.J. Bard, J. Am. Chem. Soc. 99 (1977) 7729–7731.
[10] B. Kraeutler, A.J. Bard, J. Am. Chem. Soc. 100 (1978) 2239–2240.
[11] B. Kraeutler, C.D. Jaeger, A.J. Bard, J. Am. Chem. Soc. 100 (1978) 4903–4905.
[12] T. Sakata, T. Kawai, K. Hashimoto, J. Phys. Chem. 88 (1984) 2344–2350.
[13] G.R. Dey, K.K. Pushpa, Res. Chem. Intermed. 32 (2006) 725–736.
[14] Q. Ling, J. Sun, Q. Zhou, H. Ren, Q. Zhao, Appl. Surf. Sci. 254 (2008) 6731–6735.
[15] M. Zhou, J. Yu, B. Cheng, J. Hazard. Mater. B 137 (2006) 1838–1847.
[16] W.C. Hung, Y.C. Chen, H. Chu, T.K. Tseng, Appl. Surf. Sci. 255 (2008) 2205–2213.
[17] M.A. Khan, S.I. Woo, O.B. Yang, Int. J. Hydrogen Energy 33 (2008) 5345–5351.
[18] W.S. Tung, W.A. Daoud, ACS Appl. Mater. Interfaces 1 (2009) 2453–2461.
[19] M.I. Litter, J.A. Navío, J. Photochem. Photobiol. A 98 (1996) 171–181.
[20] M.H. Zhou, J.G. Yu, B. Cheng, H.G. Yu, Mater. Chem. Phys. 93 (2005) 159–163.
[21] Y.R. Smith, K.J.A. Raj, V. Subramanian, B. Viswanathan, Sulfated Fe_2O_3–TiO_2 synthesized from ilmenite ore: a visible light active photocatalyst, Colloid Surf. A: Physicochem. Eng. Aspects 367 (2010) 140–147, doi:10.1016/j.colsurfa.2010.07.001.
[22] K.T. Ranjit, B. Viswanathan, J. Photochem. Photobiol. A 108 (1997) 79–84.
[23] S. Zhu, Y. Li, C. Fan, D. Hang, W. Liu, Z. Dun, S. Wei, Physica B 364 (2005) 199–205.
[24] G. Colón, J.M. Sánchez-España, M.C. Hidalgo, J.A. Navío, J. Photochem. Photobiol. A 179 (2006) 20–27.
[25] Z. Ambrus, N. Balázs, T. Alapi, G. Wittmann, P. Sipos, A. Dombi, K. Mogyorósi, Appl. Catal. B 81 (2008) 27–37.
[26] J. Zhu, W. Zheng, B. Hea, J. Zhang, M. Anpo, J. Mol. Catal. A 216 (2004) 35–43.
[27] H. Yoneyama, Y. Takao, H. Tamura, A.J. Bard, J. Phys. Chem. 87 (1983) 1417–1422.
[28] D. Muggli, J.L. Falconer, J. Catal. 187 (1999) 230–237.
[29] Y. Honghui, Y. Chen, L. Guo, Catal. Commun. 11 (2010) 1099–1103.
[30] A. Patsoura, D.I. Kondarides, X.E. Verykios, Catal. Today 124 (2007) 94–102.
[31] I.K. Konstantinou, T.A. Albanis, Appl. Catal. B 49 (2004) 1–14.
[32] Z. Liu, X. Zhang, S. Nishimoto, T. Murakami, A. Fujishima, Environ. Sci. Technol. 42 (2008) 8547–8551.
[33] I. Sopyan, M. Watanabe, S. Murasawa, K. Hashimoto, A. Fujishima, J. Photochem. Photobiol. A 98 (1996) 79–86.
[34] A. Kudo, Y. Miseki, Chem. Soc. Rev. 38 (2009) 253–278.
[35] H.J. Choi, M. Kang, Int. J. Hydrogen Energy 32 (2007) 3841–3848.
[36] J. Bandara, C.P.K. Udawatta, C.S.K. Rajapakse, Photochem. Photobiol. Sci. 4 (2005) 857–861.
[37] V. Gombac, L. Sordelli, T. Montini, J.J. Delgado, A. Admski, G. Adami, M. Cargnello, S. Bernal, P. Fornasiero, J. Phys. Chem. A 114 (2010) 3916–3925.
[38] S.P. Kamble, S.B. Sawant, V.G. Pangarkar, Ind. Eng. Chem. Res. 42 (2003) 6705–6713.
[39] S. Kaneco, M. Arifur Rahmana, T. Suzuki, H. Katsumata, K. Ohta, J. Photochem. Photobiol. A 163 (2004) 419–424.
[40] S. Malato, P. Fernández-Ibáñez, M.I. Maldonado, J. Blanco, W. Gernjak, Catal. Today 147 (2009) 1–59.
[41] M.N. Chong, B. Jin, Ch.W.K. Chow, Ch. Saint, Water Res. 44 (2010) 2997–3027.
[42] J.A. Navío, G. Colón, M.I. Litter, G.N. Bianco, J. Mol. Catal. A 106 (1996) 267–276.